

NUMERICAL MODELING OF FLUID-STRUCTURE INTERACTION OF A 3D WEDGE DURING WATER IMPACT WITH VARIATION OF VELOCITY AND PITCH ANGLE

F. Valpiani^{1*}, P. Cicolini¹, D. Esposto¹, A. Galletti¹ & D. Guagliardo¹

¹ Department of Mechanical and Aerospace Engineering, Polytechnic of Turin, Turin.

* teams55.polito@gmail.com

Abstract

Dynamic interactions related to structures impacting water are a very complex problem to simulate numerically due to the multi-physics interaction between fluid and structure. Seaplanes, racing boats, re-entry modules, and transport aircraft ditching are some examples of the areas that could benefit from Fluid-Structure Interaction (FSI) analyses.

The aim of the present work is to extend the previously analysed scenarios [1] of the three-dimensional structure by investigating the effects of water impacts with different initial conditions. In detail, it has been investigated the influence of horizontal velocity and pitch angle on the dynamic pressure profiles developed at impact. The analysis involves the development of a numerical model based on the explicit computational capabilities of the multi-purpose LS-DYNA software. The purpose is to generate a full impact case study useful for the evaluation of possible structural failure criteria.

The results of this kind of analyses would provide a better understanding of the impact phenomenon and enhance the structural design of the components in contact with water and subject to the impact generated stresses.

Keywords: Fluid-Structure Interaction, LS-DYNA, Smoothed Particle Hydrodynamics, FSI

List of Symbols

Symbol	Remarks
θ	Pitch Angle; angle between the X axis and the horizon
ϕ	Roll Angle; angle between the Y axis and the horizon
ψ	Yaw Angle; angle between the Z axis and the horizon
q	Pitch; angular velocity with respect to the X axis
p	Roll; angular velocity with respect to the Y axis
r	Yaw; angular velocity with respect to the Z axis
V_z	Vertical velocity component on Z axis
V_y	Horizontal velocity component on Y axis

1. Introduction

Team S55 was founded in February 2017 by a group of students from the DIMEAS department of the Politecnico di Torino. The team's goal is to reproduce a 1:8 scale flying version of the historic SIAI-Marchetti S55X seaplane by taking advantage of modern engineering approaches [2, 3]. The work presented here is carried out by the Fluid-Structure Interaction division, which aims to

numerically model the water impact of the hull using LS-DYNA software. The typical approach of approximating the geometry of a generic hull to the geometry of a 2D wedge is generally adopted for all studies of this type. This method was initially developed by von Kármán [4] and later extended with Wagner's analytical theory [5].

The analytical approach shows that the pressure generated at impact is strongly influenced by the hull's dihedral angle and the vertical impact velocity. These behaviours have been investigated by previous studies [1, 6] carried out at the Politecnico di Torino. In these works, a numerical model was proposed that could predict the pressure profile developed as function of the dihedral angle and vertical impact velocity. The models under discussion involved the use of a two-dimensional geometry for the structural part. The impact solved in this way was able to simulate only the vertical force and eliminates the interactions along the wedge length; on the other hand, it allows to evaluate the influence of the dihedral angle on the maximum pressures developed at impact. A three-dimensional structure was subsequently proposed [1] to reproduce the impact phenomenon encompassing 3D effects and interactions. The vertical drop performance on the global 3D model (which demands a lower computational requirement) was then compared with the higher detailed and accurate 2D local model (which is associated with a high computational cost). Table 1 shows the results of the previous comparison between the 2D and 3D models; these values were used to validate the performance of the model under discussion in the present work. In the paper [6] we point out the critical key-point of this kind of experimentation by proposing the design of a preliminary experimental impact test.

The numerical model used is based on the explicit computational capabilities of the multi-purpose LS-DYNA software. The tank and the wedge are the two components of the simulation. The numerical modelling of the tank has an inherent complexity due to the fluid material that is subject to large deformation fields and high-pressure gradients. Therefore, the conventional FEM elements are not useful for this type of simulation. LS-DYNA provides a few possible alternatives for FSI simulation including the Arbitrary Lagrangian-Eulerian ALE-Method, the Smoothed Particle Hydrodynamics SPH-method, and the Incompressible Computational Fluid Dynamics ICFD-method. In our studies we proceeded with the SPH formulation. This type of element can be visualized as a sphere containing a finite volume of water. The characteristic size of the SPH element is the diameter which will also control the computational cost associated with the analysis. Therefore, for a given volume, the larger the diameter of the SPH element the smaller will be the number of elements used and the lower the computational cost. So, the calibration of the fluid element size is done by considering the size of the structural SHELL element. From the previous evaluations [1], it turns out that in order to have a good accuracy the single SHELL element must come in contact with at least one SPH element.

2. Model

The impact system consists of a rigid wedge and an SPH-filled tank. The wedge geometry has been modified from previous work [1] to achieve a more hull-like interaction with water during impact. The system dimensions are shown in Figure 1. The wedge mechanical properties are those of a generic steel alloy, simulated through the LS-Dyna Keyword MAT_RIGID; with reference to the coordinate system in Figure 1 (bottom), translational degrees of freedom along the X-axis and rotations around the Y-axis and Z-axis are locked.

The tank geometry shown in Figure 1 (bottom) is calibrated in the longitudinal direction, along the Y-axis, to ensure the correct simulation of the wedge with non-zero horizontal velocity. Increasing the tank volume requires a greater number of SPH elements, which results in higher computational cost, or an increase in their characteristic size, which result in coarser spatial resolution. To enable the execution of the simulation in personal computers the total number of elements is kept below the threshold of 100 thousand elements: in fact, the total number of SPH elements is 96,000, while the

SHELL elements are 2,068. The containment structure of SPH elements is managed by 5 keywords RIGIDWALL_PLANAR. The reference axes of the wedge-tank system are oriented according to the triad shown in Figure 1 (below).

The pressure profile on the wedge surface is acquired in six regions, by the sensor P1 through sensor P6, distributed according to Figure 1 (top). Sensors P1 and P2 are placed on the centre of the wedge sagittal plane to allow direct comparison with the results previously validated in the paper [1].

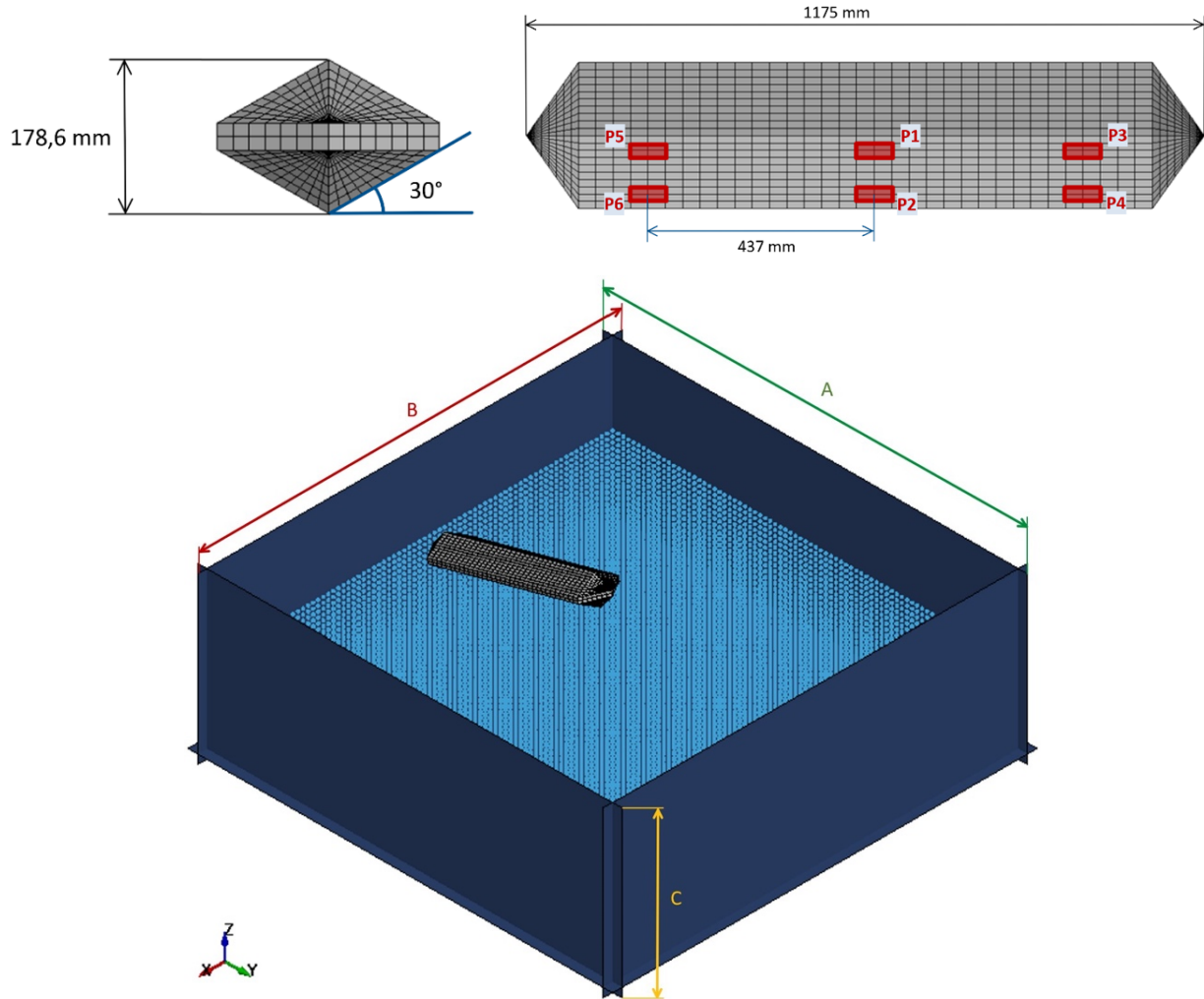


Figure 1 – Impact System Sensors (top) and geometry (bottom). A = 2600 mm, B = 2600 mm, C = 800 mm.

Test Case	Acceleration Peak [G] - Time Step [ms]	Peak Pressure [MPa] – Time Step [ms]
LOCAL (2D) [1]	10.8 G – 9.20 ms	0.089 G – 2.90 ms
GLOBAL (3D) [1]	11.7 G – 10.9 ms	0.105 G – 7.90 ms
VALIDATION	10.9 G – 18.0 ms	0.150 G – 8.30 ms

Table 1 – Peak acceleration comparison with previous work [1].

Table 1 shows the acceleration and pressure peaks obtained for preliminary validation of the present model. Changes can be found regarding the ratio between SHELL elements size and SPH elements size. In the previous study, a higher density of SPH could be achieved due to the smaller tank volume necessary to simulate an impact with only the vertical velocity. The single sensor used consists of 9 SHELL elements for a total area of 40 cm².

The remaining four sensors, shown in Figure 1 (top), were placed as follows: two near the stern (P3 and P4) and two near the bow (P5 and P6). Specifically, sensors P1, P3 and P5 are placed at 18 mm to the wedge apex, while sensors P2, P4 and P6 are placed at 64 mm from the vertex. The thickness of SHELL elements is 2 mm with 3 integration points. The complete wedge structural mass is 11 kg, to which a non-structural mass is added to stabilize the numerical solution as presented in [1].

3. Test Case

The purpose of this parametric investigation is to understand the influence of the horizontal velocity V_Y and pitch angle θ on the quantities of interest. Considering the expected landing conditions of the S55 seaplane under study, the following initial pitch angle and horizontal velocity values were selected:

$$\theta = 0^\circ ; 10^\circ ; 20^\circ$$

$$V_Y = 0 \text{ m/s} ; 5 \text{ m/s} ; 10 \text{ m/s}$$

$$V_Z = -5 \text{ m/s}$$

For a total of 9 simulations carried out with constant vertical speed of -5m/s. The quantities of interest for studying a real landing scenario are the wedge accelerations and pressures on the wedge surface. The simulation data were collected in 2 sets of graphs to study the influence of θ and horizontal velocity V_Y on the quantities of interest. In addition, to get confirmations on the accuracy of the simulations carried out, linear velocities V_Y , V_Z , angular velocities ω and angle variation were also diagrammed. Table [2] sums up all the analysed scenarios:

$\theta = 0^\circ$ $\theta = 10^\circ$ $\theta = 20^\circ$	$V_Y = 0 \text{ m/s}$	$V_Y = 5 \text{ m/s}$	$V_Y = 10 \text{ m/s}$	TEST CASE A
$V_Y = 0 \text{ m/s}$ $V_Y = 5 \text{ m/s}$ $V_Y = 10 \text{ m/s}$	$\theta = 0^\circ$	$\theta = 10^\circ$	$\theta = 20^\circ$	TEST CASE B

Table 2 – Analysed Test Cases.

4. Data Acquisition and Processing

The data obtained from the numerical analysis has been exported from LS-Dyna for further processing. It has been noted that the obtained signals contain significant noise: repeated simulations have shown that this is increased by further coarsening of the spatial discretization, suggesting that such noise may be related to the low number of SPH used. Past publications [1] have been focused on low computational cost simulations and as such a noisy signal is to be

expected. The numerical data from simulations have been filtered by a Butterworth filter with a 180 Hz cut-off frequency. To avoid the expected phase distortion typical of an Infinite Impulse Filter we implemented a forward-backward filtering. This approach ensures zero-phase filtering at the cost of having a non-causal filter which is not suited for real time applications. This drawback was considered acceptable as we focus on low computational cost and offline post processing. The wedge angular velocity has been calculated by numerical differentiation of the pitch angle filtered time history signal. This approach ensures low computational cost paired with reasonable accuracy compared to other, more sophisticated methods [7].

5. Results

The results of the performed parameterizations are presented according to the scheme in Table 2.

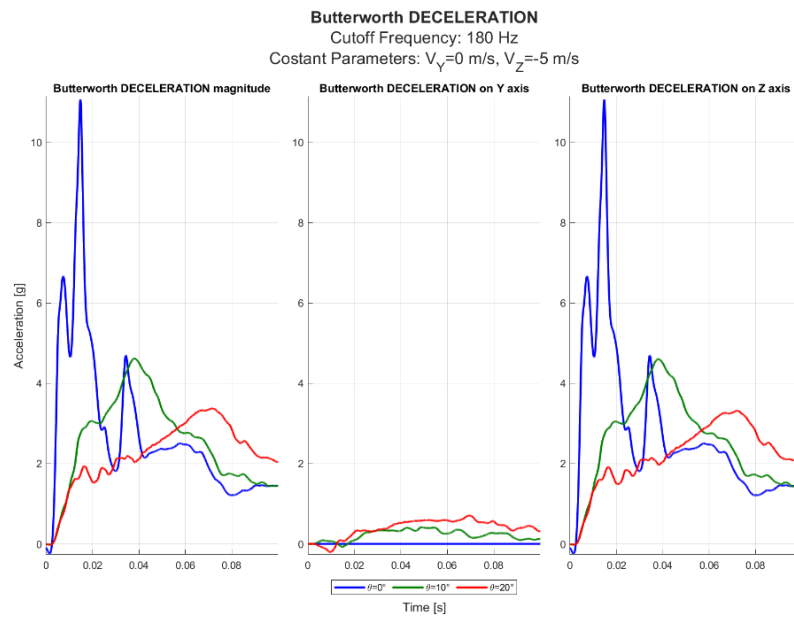


Figure 2 – Acceleration, pitch angle variation:
 $p = r = 0$ rad/s ; $V_X = V_Y = 0$ m/s ; $V_Z = -5$ m/s.

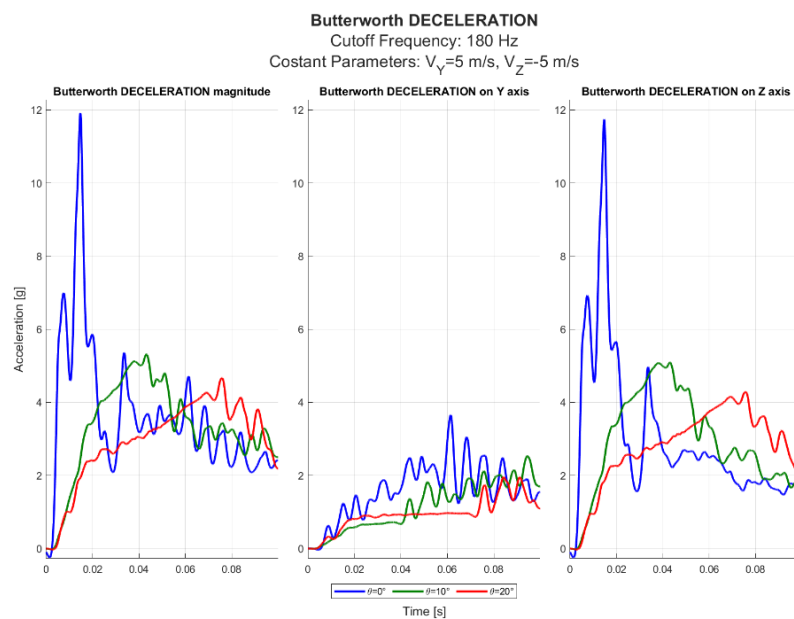


Figure 3 – Acceleration, pitch angle variation:
 $p = r = 0$ rad/s ; $V_X = 0$ m/s ; $V_Y = 5$ m/s ; $V_Z = -5$ m/s.

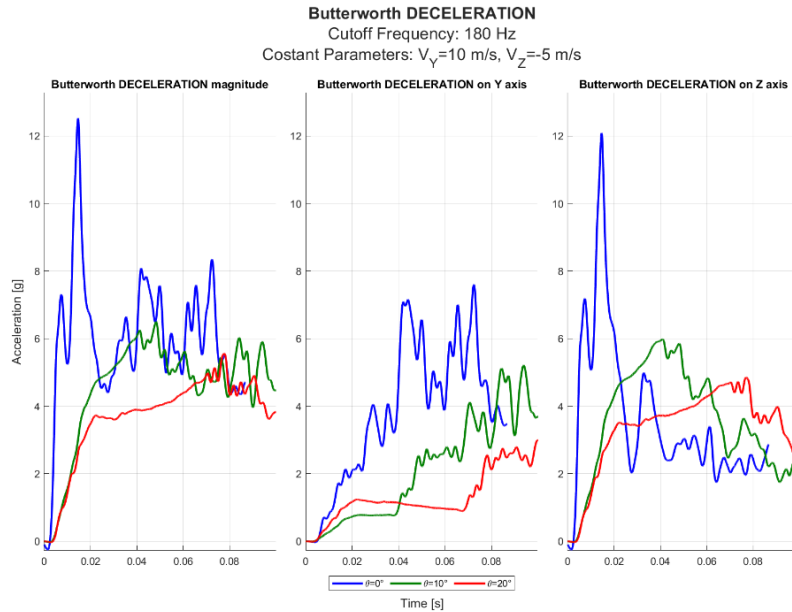


Figure 4 – Acceleration, pitch angle variation:
 $p = r = 0$ rad/s; $V_X = 0$; $V_Y = 10$ m/s; $V_Z = -5$ m/s.

The influence of the initial θ on the wedge acceleration profile is illustrated for TEST CASE A. In detail, Figure 2 shows the resulting acceleration profiles, horizontal and vertical accelerations for the case in which the wedge impacts the free water surface without an initial horizontal velocity. It is observed that for zero horizontal velocities and zero θ , there is no acceleration in the Y direction which means that the impact is perfectly vertical. As pitch increases, the peak deceleration decreases from about 10 g for $\theta = 0^\circ$ to less than 4 g for $\theta = 20^\circ$, resulting in a decrease of about 6 g. In contrast, as the pitch angle increases, there is an increase in the deceleration component along the Y-axis, which is zero in the case of $\theta = 0^\circ$.

Figure 3 shows the case where the initial horizontal velocity is 5 m/s. As the pitch increases, the deceleration peak decreases from about 11 g for $\theta = 0^\circ$ to about 5 g for $\theta = 20^\circ$, resulting in a decrease of about 6 g as in the previous case. A difference from the previous case is that the deceleration component along y is always non-zero and again decreases as pitch increases from 3.5 g for $\theta = 0^\circ$ to 2 g for $\theta = 20^\circ$.

Figure 4 shows the case where the initial horizontal velocity is 10 m/s, and similar considerations apply to those made for Figure 3. However, it can be seen that because of the higher horizontal velocity, the peak of a_Y is offset by about 25 ms from the peak of the a_Z component. This explains why the peak of the resultant acceleration does not deviate much from that recorded on the single component along Z. In conclusion as the initial pitch angle θ increases a decrease in the deceleration magnitude can be observed for any value of the initial horizontal velocity. This effect is related to the reduction in Fluid-Structure contact surface area as θ increases.

Figure 5, 6 and 7 shows the dynamic profiles of the pressures: three curves are shown in each graph, with pitch angle variation and constant horizontal velocity. Figure 5 shows the pressure profiles of the six sensors for the case in which the wedge impacts with a zero-horizontal velocity. It is evident that for $\theta = 0^\circ$ the pressures recorded by the six sensors are the same. The peak is reached for $t \cong 12$ ms and is approximately 0.16 MPa. Note that sensors 1, 3, 5 are wetted before sensors 2, 4, 6 since they are placed closer to the wedge apex. As the pitch angle θ increases, sensors located in the stern (sensors 3 and 4) will impact first, followed by sensors 1 and 2 (in the centreline) and finally sensors 5 and 6 located in the bow. So, the peak pressure will be the more out-of-phase the greater the pitch angle. Together with the phase shift, there is also a decrease in peak pressure as the pitch

angle θ increases. For example, with reference to sensor 1, a reduction of about 50 percent is observed.

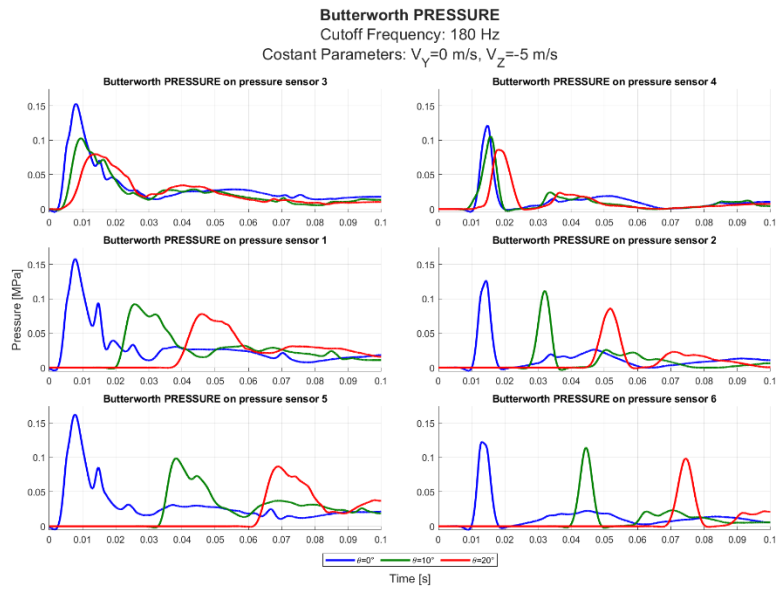


Figure 5 – Pressures, pitch angle variation:
 $p = r = 0$ rad/s; $V_X = V_Y = 0$ m/s; $V_Z = -5$ m/s.

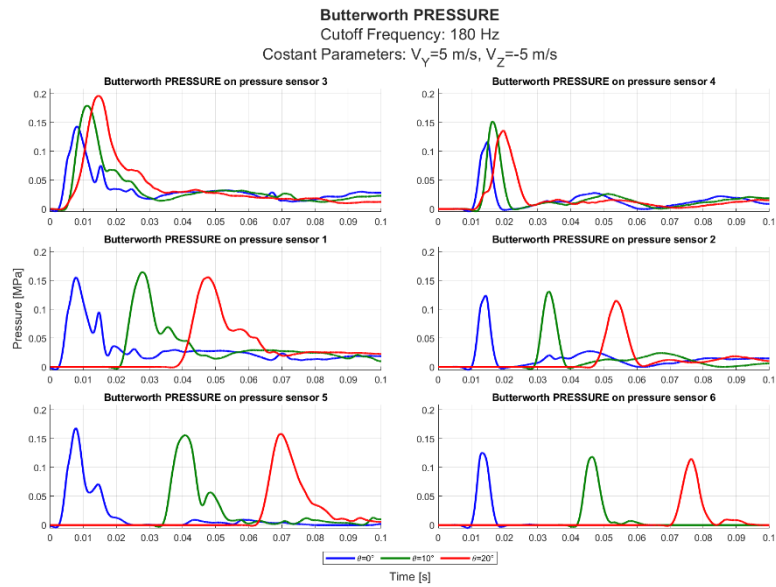


Figure 6 – Pressures, pitch angle variation:
 $p = r = 0$ rad/s; $V_X = 0$ m/s; $V_Y = 5$ m/s; $V_Z = -5$ m/s.

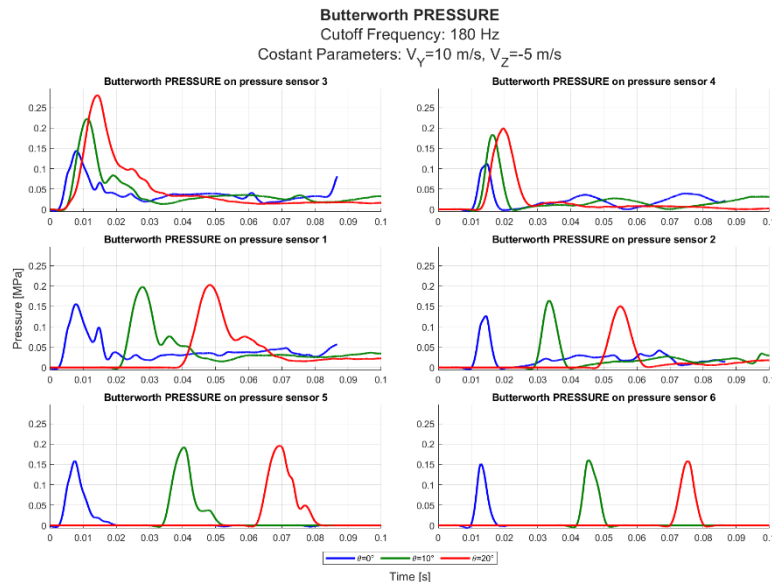


Figure 7 – Pressures, pitch angle variation:
 $p = r = 0$ rad/s ; $V_X = 0$ m/s ; $V_Y = 10$ m/s ; $V_Z = -5$ m/s.

Figure 6 shows the case where the impact is performed with a horizontal velocity of 5 m/s. In this case, there is an inversion of the previous case trend in sensors 3 and 4: the pressure increases as the pitch angle θ increases.

Further increasing the horizontal speed to 10 m/s the phenomenon becomes more noticeable. In Figure 7 an increase in pressure in each of the sensors can be observed as the θ increases. For sensors P3 and P4, located in the stern area, the increase in peak pressure is about 50%. The increase in pressure also occurs in the centre and bow sensors, although it is less pronounced it constitutes a change in trend compared to the case with zero horizontal velocity.

Regarding the accelerations and pressures profiles recorded with variation of horizontal velocity, it can be concluded that increasing the θ results in:

- a decrease in acceleration, and thus a decrease in inertial loads on the structure. This has a beneficial effect by lowering the stresses on the structural components.
- an overall increase in peak pressure, particularly in the stern area. This obviously has a negative effect as it results in higher localized loads, with greater risk of cracks and delamination.

An important effect of impact in water with non-zero pitch angle θ is played by the angular momentum, which tends to bring the structure back to a horizontal position. In the present study, this effect is therefore evaluated by calculating the angular velocity as the pitching angle changes. The linear velocity and angular velocity graphs are shown in Figure 8. At $t=0$ the velocity magnitude is expressed as the composition of horizontal and vertical velocity. Figure 8 shows the most significant results obtained with initial horizontal velocity of 5 m/s and initial vertical velocity of -5 m/s.

Following the impact, a decrease in the absolute value of the Y and Z velocity components can be observed as expected. The angular velocity is different in all the considered scenarios: as a matter of fact, even if $\theta_-(t=0)=0^\circ$ an initial horizontal velocity $V_Y \neq 0$ causes an asymmetrical pressure distribution. This effect can result in an increase in the pitch angle θ of the wedge that can raise the bow area.

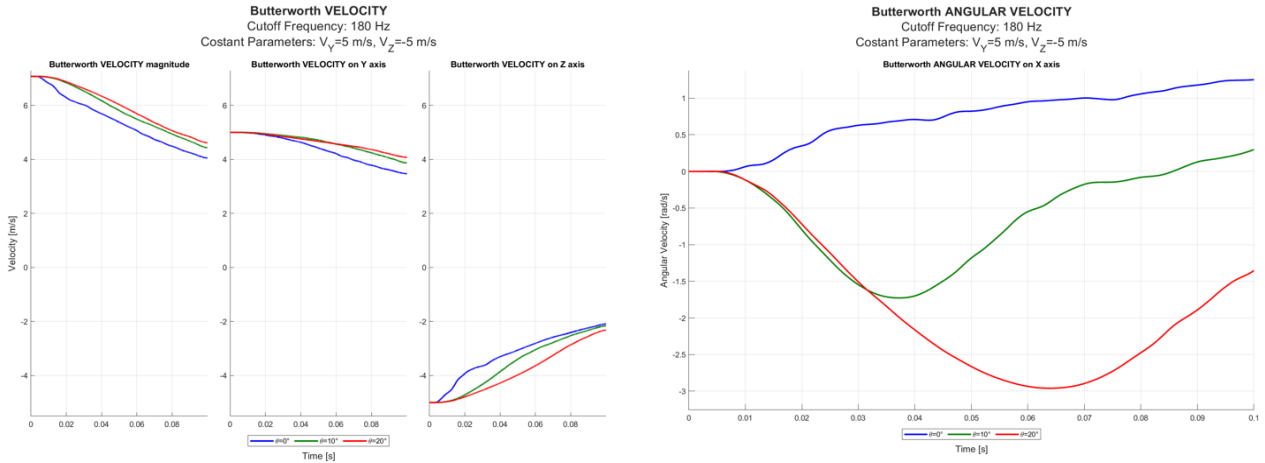


Figure 8 – Linear (left) and angular (right) velocities, pitch angle variation:
 $p = r = 0 \text{ rad/s}$; $V_X = 0 \text{ m/s}$; $V_Y = 5 \text{ m/s}$; $V_Z = -5 \text{ m/s}$.

For $\theta_{t=0} \neq 0^\circ$ the impact triggered rotation has a negative sign as the impacting stern is slowed down. When the bow is wetted, the pressure peak observable on pressure sensors P5 and P6 in Figure 6 triggers positive angular velocity slows negative rotation. This is clearly observable when the initial pitch angle θ increases.

The influence of horizontal velocity on the wedge acceleration profile is illustrated for TEST CASE B in the following images.

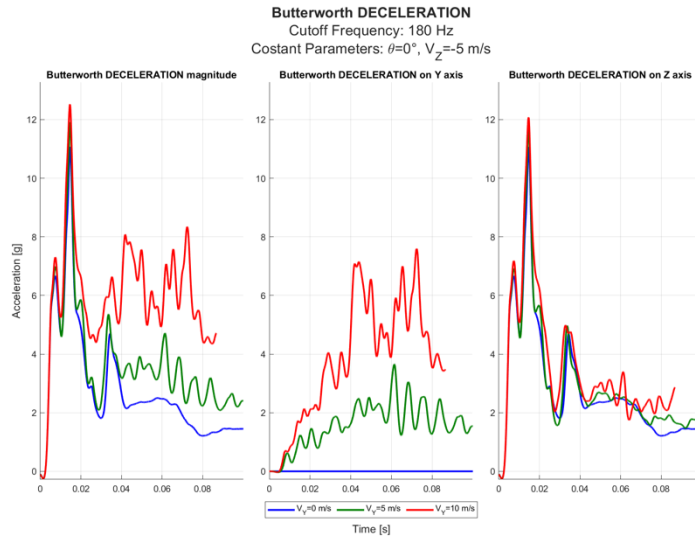


Figure 9 – Acceleration, horizontal velocity variation:
 $\theta = 0^\circ$; $p = r = 0 \text{ rad/s}$; $V_X = 0 \text{ m/s}$; $V_Z = -5 \text{ m/s}$.

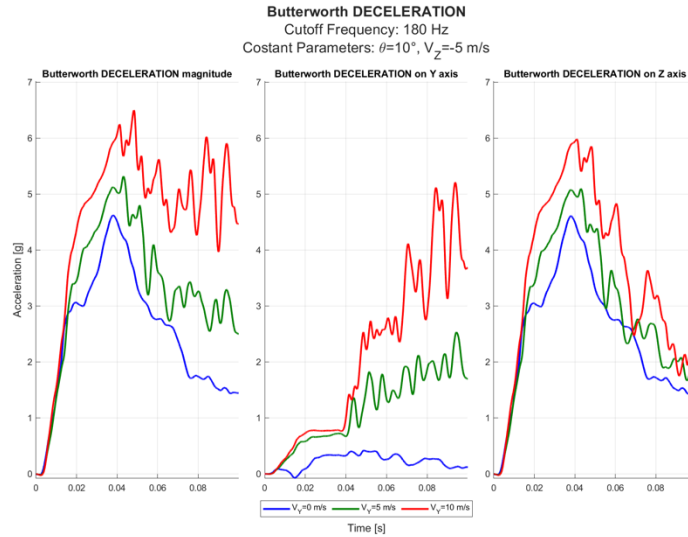


Figure 10 – Acceleration, horizontal velocity variation:
 $\theta = 10^\circ$; $p = r = 0$ rad/s ; $V_X = 0$ m/s ; $V_Z = -5$ m/s.

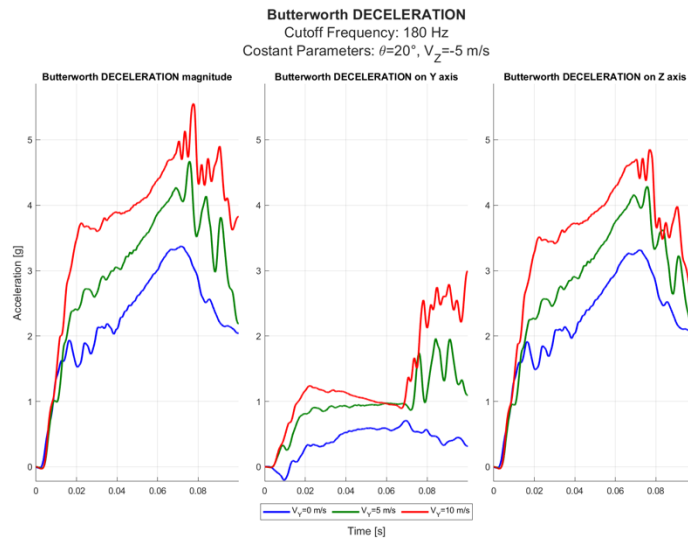


Figure 11 – Acceleration, horizontal velocity variation:
 $\theta = 20^\circ$; $p = r = 0$ rad/s ; $V_X = 0$ m/s ; $V_Z = -5$ m/s.

In Figure 9 it is observed that for the case with zero $\theta_{t=0}$, as V_Y increases, the a_Y component increases, while the a_Z component remains almost unaffected by the increase in horizontal velocity. The deceleration peak along Y, located between 40 and 80 ms is delayed in comparison with the deceleration peak along Z, located at about 20 ms.

In Figure 10 it is evaluated the case with $\theta_{t=0}=10^\circ$. There is an increase in acceleration in both the Y-axis and Z-direction as V_Y increases, this also results in an increase in the resultant acceleration from 4.5 g in the case of $V_Y = 0$ m/s to 6 g in the case of $V_Y = 10$ m/s . Increasing the $\theta_{t=0}$ to 20° in Figure 11 a similar trend to the previous case is shown. Both the Y and Z acceleration components increase as V_Y increases. The peak of the resultant acceleration increases from 3.5 g in the case $V_Y = 0$ m/s to 5.5 g in the case $V_Y = 10$ m/s. Thus, a reduction in the peak deceleration is seen as the $\theta_{t=0}$ increases; this phenomenon is attributed to a smaller SHELL-SPH contact surface due to the greater pitch of the wedge.

The next figures will show the dynamic pressure profiles by organizing them as in the previous case: three curves are shown in each graph, with horizontal velocity variation and constant θ .

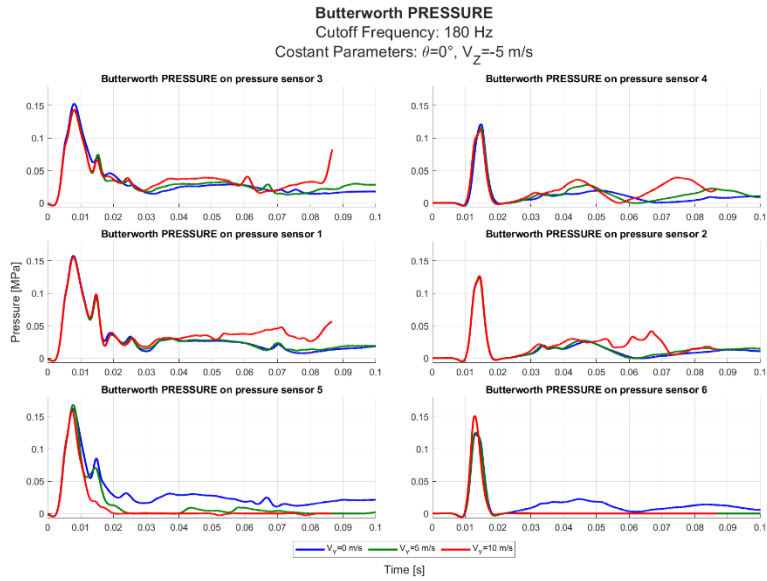


Figure 12 – Pressures, horizontal velocity variation:
 $\theta = 0^\circ$; $p = r = 0$ rad/s ; $V_x = 0$ m/s ; $V_z = -5$ m/s.

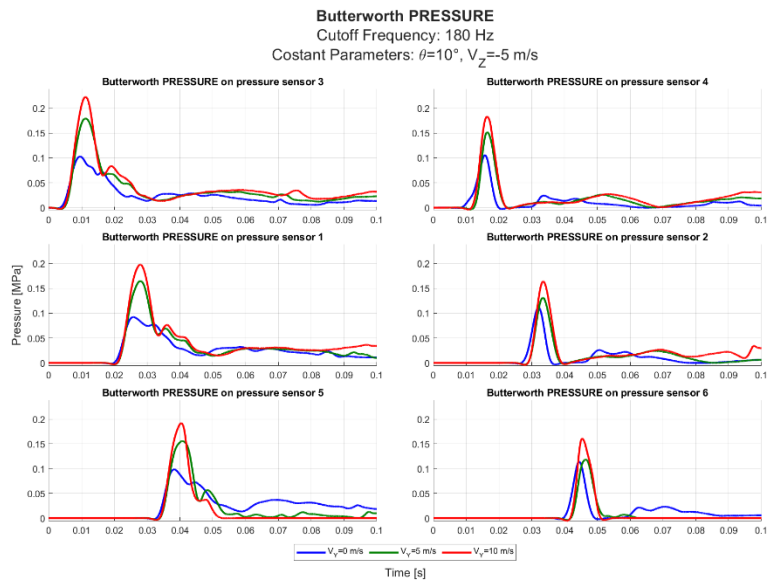


Figure 13 – Pressures, horizontal velocity variation:
 $\theta = 10^\circ$; $p = r = 0$ rad/s ; $V_x = 0$ m/s ; $V_z = -5$ m/s .

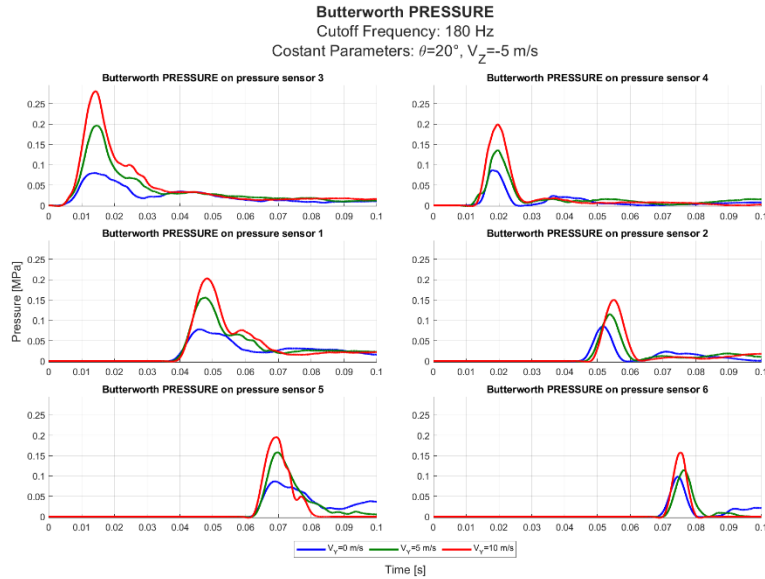


Figure 14 – Pressures, horizontal velocity variation:
 $\theta = 20^\circ$; $p = r = 0$ rad/s; $V_x = 0$ m/s; $V_z = -5$ m/s.

In Figure 12 the pressure peaks recorded by the six sensors show no appreciable change as V_y increases, in fact for $\theta_{t=0} = 0^\circ$ the sensor's impact at the same time. The maximum peak pressure is about $p_{max} \cong 0.15$ MPa.

In contrast to the previous case in Figure 13 with $\theta = 10^\circ$, as V_y increases, the peak pressure increases. The maximum pressure is recorded by sensor 3, where it goes from $p_{max} \cong 0.11$ MPa for $V_y = 0$ m/s to $p_{max} \cong 0.25$ MPa for $V_y = 10$ m/s.

Figure 14 shows the trends of pressures obtained with $\theta_{t=0}$ of 20° . The trend is similar to the previous one, the maximum pressure in this case goes from $p_{max} \cong 0.08$ MPa for $V_y = 0$ m/s up to $p_{max} \cong 0.3$ MPa for the $V_y = 10$ m/s case.

In conclusion, in terms of pressure, the impact performed with increasing $\theta_{t=0}$ and with increasing velocities can cause a strong increase in the peak pressure acting on the structure.

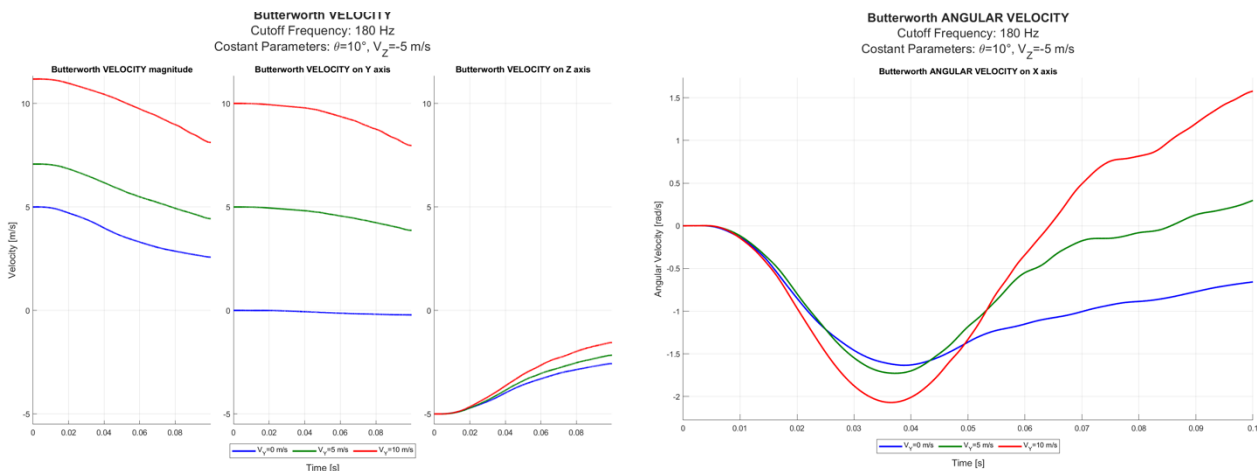


Figure 15 – Linear (left) and angular (right) velocities, horizontal velocity variation:
 $p = r = 0$ rad/s; $V_x = 0$ m/s; $\theta = 20^\circ$; $V_z = -5$ m/s.

For linear and angular velocities, it was chosen, as a representative case, the one with an initial pitch angle θ of 10° shown in Figure 15. As the θ is greater than 0° following impact, a negative pitch velocity develops, which pulls the wedge back into horizontal position.

After reaching an overall minimum, the angular velocity tends to decrease in modulus until it changes sign in the cases with non-zero horizontal velocity, generating a flotation condition of the wedge. In the case with zero horizontal velocity, the angular velocity profile tends to gradually extinguish until a condition of horizontal equilibrium is reached.

6. Conclusions

The study presented is an extension of the previously published results [1]. In this work, the investigation is enriched by evaluating the influence of horizontal velocity and θ on dynamic acceleration and pressures at impact. It is shown that for the ranges evaluated, in general the increase in horizontal velocity does not greatly affect the acceleration peaks; on the other hand, the pressure is found to be strongly dependent on the horizontal velocity, and the peak increases are more pronounced for the higher the θ at impact. This type of evaluation helps to better understand the dynamics that develop upon impact in water of a rigid wedge and can be easily extended to different geometries and materials.

Referring to Figure 16, the next steps involve modelling additional complexities:

1. Geometry of real hulls of the S55X with an evaluation of wave reflection between the two hulls
2. Evaluation of the influence of roll angle ϕ and a transverse horizontal velocity V_x directed along X-axis.
3. Modelling of the inertias of the complete seaplane.

This will provide a complete simulation of the Savoia-Marchetti S55X aircraft hulls, and it will be possible to identify the areas with the greatest load to optimize and properly size the optimized design configuration of the hulls.

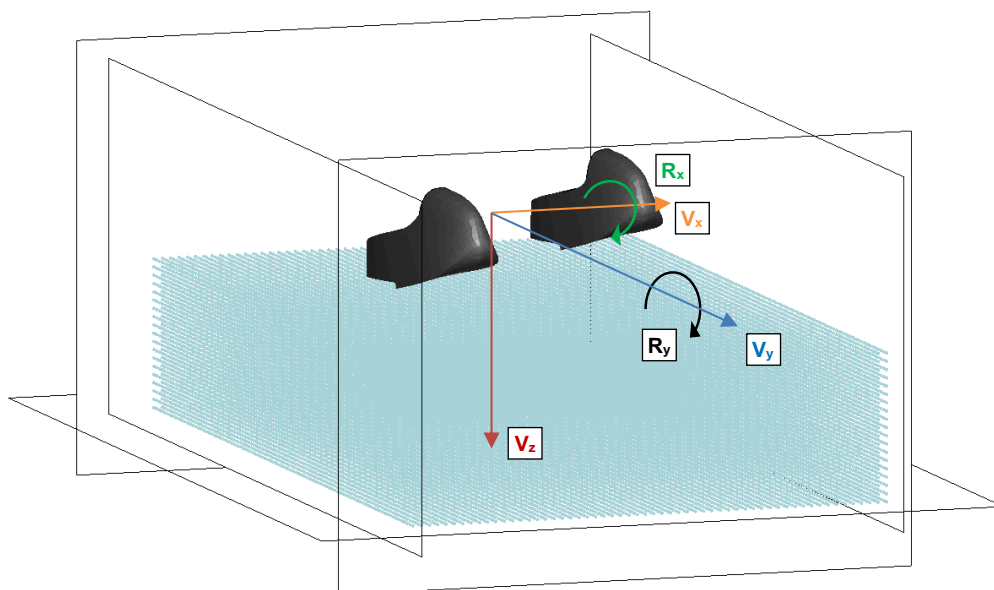


Figure 16 – Future Work Geometry, Initial velocity, and rotations.

7. Acknowledgment

The authors thank Professor Cestino and Engineer Sapienza for their support and guidance. In addition, we would like to thank the Politecnico di Torino and the DIMEAS department for the provision of resources and facilities.

8. Copyright Statement

The authors confirm that they, and/or their company or organization, hold copyright on all the original material included in this paper. The authors also confirm that they have obtained permission, from the copyright holder of any third-party material included in this paper, to publish it as part of their paper. The authors confirm that they give permission or have obtained permission from the copyright holder of this paper, for the publication and distribution of this paper as part of the ICAS proceedings or as individual off-prints from the proceedings.

References

- [1] Valpiani F, Polla A, Cicolini P, Grilli G, Cestino E, Sapienza V. Early Numerical Evaluation of Fluid-Structure Interaction of a Simply Wedge Geometry with Different Deadrise Angle. *AIDAA XXVI International Congress*, Pisa, 2021.
- [2] Cestino E, Frulla G, Sapienza V, Pinto P, Rizzi F, Zaramella F, Banfi D. Replica 55 Project: A Wood Seaplane in The Era of Composite Materials. *ICAS 2018 31st Congress of The International Council of the Aeronautical Sciences*, Belo Horizonte, 2018.
- [3] Loiodice L, Brugnera A, Di Cosmo D, Di Domenico V, Fallucca R, Grendene S, Piani R, Prodan M. Design and Building a 1:8 Scale Replica of the SIAI Marchetti S55X. *AIDAA XXVI International Congress*, Pisa, 2021.
- [4] von Kármán T. The impact on seaplane floats during landing. *NACA Technical Notes N.321*, 1929.
- [5] Wagner H. Über Stoß- und Gleitvorgänge an der Oberfläche von Flüssigkeiten. *Zeitschrift Für Angewandte Mathematik Und Mechanik*, Vol. 12, No. 4, 1932.
- [6] Nicolosi G, Valpiani F, Grilli G, Saponaro Piacente A, Di Ianni L, Cestino E, Sapienza V, Polla A, Piana P. Design of a Vertical Ditching Test. *ICAS 2020 32nd Congress of the International Council of the Aeronautical Sciences*, Shanghai, 2020.
- [7] van Breugel F V, Kutz J N, Brunton B W. Numerical differentiation of noisy data: A unifying multi-objective optimization framework. *IEEE Access*, Vol. 8, 2020.